PHYSICAL REVIEW D **76,** 104051 (2007)

Chaos in a three-body self-gravitating cosmological spacetime

M. J. Koop* and R. B. Mann†
Department of Physics, University of Waterloo, Waterloo, Ontario N2L 3G1, Canada

S. Bachmann‡
Institute for Theoretical Physics, ETH Zurich, 8093 Zurich, Switzerland
(Received 29 May 2006; revised manuscript received 7 September 2007; published 30 November 2007)

We investigate the equal-mass three-body system in general relativistic lineal gravity in the presence of a cosmological constant Λ. The cosmological vacuum energy introduces features that do not have a nonrelativistic counterpart, inducing an expansion/contraction of space-time that competes with the gravitational self-attraction of the bodies. We derive a canonical expression for the Hamiltonian of the system and discuss the numerical solution of the resulting equations of motion. As for the system with $\Lambda = 0$, we find that the structure of the phase space yields a rich variety of interesting dynamics that can be divided into three distinct regions: annulus, pretzel, and chaotic; the first two being regions of quasiperiodicity while the latter is a region of chaos. However, unlike the $\Lambda = 0$ case, we find that a negative cosmological constant considerably diminishes the amount of chaos in the system, even beyond that of the $\Lambda = 0$ nonrelativistic system. By contrast, a positive cosmological constant considerably enhances the amount of chaos, typically leading to KAM (Kolmogorov-Arnold-Moser) breakdown.

DOI: 10.1103/PhysRevD.76.104051 PACS numbers: 05.45.Ac, 04.40.−b, 04.20.Jb, 04.25.−g

I. INTRODUCTION

The N-body problem—that of describing the motion of a system of N particles interacting through specified forces—is one of the oldest problems in physics. Even now it continues to be a problem in fields ranging from nuclear physics to stellar evolution and cosmology. When the problem is that of N particles interacting through their mutual gravitational attraction it is particularly challenging. In the Newtonian case in three spatial dimensions, an exact solution is only known for the $N = 2$ case, and for the general relativistic case in three spatial dimensions there is no exact solution for the equations of motion for even the $N = 2$ case (although approximation techniques exist [1]). This is largely due to the dissipation of energy in the form of gravitational radiation, which results in the system needing to be solved by approximate solutions.

Considerable progress has been made in recent years by studying systems with reduced spatial dimensions. Nonrelativistic one-dimensional self-gravitating systems (OGS) of N particles have been very important in the fields of astrophysics and cosmology for over 30 years [2]. Although they are primarily used as prototypes for studying gravity in higher dimensions, there are physical systems with dynamics closely approximated by the one-dimensional system. Very long-lived core-halo configurations, reminiscent of structures observed in globular clusters, are known to exist in the OGS phase space [3]. These model a dense massive core in near-equilibrium, surrounded by a halo of high kinetic energy stars that interact only weakly with the core. Also, the collisions of flat parallel domain walls moving in a direction perpendicular to their surfaces and the dynamics of stars in a direction orthogonal to the plane of a highly flattened galaxy are approximated by the OGS system.

In this paper we continue an ongoing investigation into relativistic one-dimensional self-gravitating systems (ROGSs). This is carried out in the context of a $(1 + 1)$-dimensional theory of gravity (lineal gravity) that models $(3 + 1)$ general relativity by setting the Ricci scalar R equal to the trace of the stress energy of prescribed matter fields and sources. For the ROGS these sources are point particles minimally coupled to gravity. Hence, as in $(3 + 1)$ dimensions, the evolution of space-time curvature is governed by the matter distribution, which in turn is governed by the dynamics of space-time [4]. Referred to as $R = T$ theory, it is a particular member of a class of dilaton gravity theories on a line. What makes this theory of particular interest is that it has a consistent nonrelativistic ($c \to \infty$) limit [4] (a problem for generic $(1 + 1)$-dimensional gravity [5]), and in this limit reduces to the Newtonian OGS as a special case. Furthermore, when the stress energy is that of a cosmological constant, it reduces to Jackiw-Teitelboim theory [6].

The three-body ROGS has been studied previously and compared to the corresponding nonrelativistic system [7] in the case of a zero cosmological constant for both equal and unequal masses [8,9]. The degrees of freedom in both the nonrelativistic and relativistic systems can be rewritten in terms of a single particle moving in a two-dimensional potential well of hexagonal symmetry. In the nonrelativistic case the potential grows linearly as a function of radial

*mjkoop@sciborg.uwaterloo.ca
†rbmann@sciborg.uwaterloo.ca
‡svenb@phys.ethz.ch

distance, but in the relativistic case the growth is nonlinear, yielding a potential in the shape of a hexagonal carafe. For both systems, two broad categories of periodic and quasi-periodic motion were found, referred to as annulus and pretzel orbits, as well as a set of chaotic motions appearing in the phase space between these two types. The phase space between the two systems was found to be qualitatively the same despite the high degree of nonlinearity in the relativistic system.

In this paper we study the three-body ROGS with nonzero cosmological constant Λ. This situation has no nonrelativistic analogue. The effect of the cosmological constant is to induce an expansion/contraction of spacetime that competes with the gravitational self-attraction of the bodies. This system has been studied in some detail in the case of two interacting bodies, and it has been shown that relativistic effects are considerably enhanced by the presence of Λ [10]. For example a sufficiently large and positive Λ can overcome the attraction of the bodies, which then ''lose causal'' contact over a finite amount of proper time. The effect of Λ on the chaotic behavior of the three-body system has never been studied. It is the purpose of this paper to examine this problem, restricting our investigation to the equal-mass case.

We briefly review the formalism in Sec. II of the N-body problem, obtaining the Hamiltonian of the particles in terms of their canonical degrees of freedom. We discuss our methods for solving the constraint equations in Sec. III and for solving the equations of motion in Sec. IV, defining a coordinate system that allows us to describe the three-particle system as a single particle on a plane, moving in a potential well with hexagonal symmetry. In Sec. V we present various Poincaré maps and discuss how the global phase space is distorted in the presence of a nonzero cosmological constant. We find that a negative cosmological constant considerably reduces the amount of chaotic behavior, whereas a positive cosmological constant considerably enhances it. In Sec. VI we discuss the salient features of our solutions and make some conjectures regarding their general properties. We close the paper with some concluding remarks and directions for further work.

II. CANONICAL REDUCTION OF THE N-BODY PROBLEM IN LINEAL GRAVITY

As in previous work [7–9] we begin with the action integral for the gravitational field coupled with N point particles, which is

$$I = \int d^2x \left[\frac{1}{2\kappa}\sqrt{-g}\left\{ \Psi R + \frac{1}{2} g^{\mu\nu} \nabla_\mu \Psi \nabla_\nu \Psi + \Lambda \right\} - \sum_{a=1}^{N} m_a \int d\tau_a \left\{ -g_{\mu\nu}(x) \frac{dz_a^\mu}{d\tau_a} \frac{dz_a^\nu}{d\tau_a} \right\}^{1/2} \delta^2(x - z_a(\tau_a)) \right], \tag{1}$$

where $g_{\mu\nu}$ and g are the metric and its determinant, R is the Ricci scalar, τ_a is the proper time of the ath particle, $\kappa = 8\pi G/c^4$ is the gravitational coupling, and with a scalar (dilaton) field Ψ. This action describes a generally covariant self-gravitating system (without collision terms, so that the bodies pass through each other), in which the scalar curvature is sourced by the point particles and the cosmological constant Λ. Variation of the action with respect to the metric, particle coordinates, and dilaton field yields the field equations

$$R - \Lambda = \kappa T^{P\mu}_{\mu}, \tag{2}$$

$$\frac{d}{d\tau_a}\left\{ \frac{dz_a^\nu}{d\tau_a} \right\} + \Gamma^\nu_{\alpha\beta}(z_a) \frac{dz_a^\alpha}{d\tau_a} \frac{dz_a^\beta}{d\tau_a} = 0, \tag{3}$$

$$\frac{1}{2} \nabla_\mu \Psi \nabla_\nu \Psi - g_{\mu\nu}\left(\frac{1}{4} \nabla^\lambda \Psi \nabla_\lambda \Psi - \nabla^2 \Psi \right) - \nabla_\mu \nabla_\nu \Psi = \kappa T^P_{\mu\nu} + \frac{\Lambda}{2} g_{\mu\nu}, \tag{4}$$

where the stress energy due to the point masses is

$$T^P_{\mu\nu} = \sum_{a=1}^{N} m_a \int d\tau_a \frac{1}{\sqrt{-g}} g_{\mu\sigma} g_{\nu\rho} \frac{dz_a^\sigma}{d\tau_a} \frac{dz_a^\rho}{d\tau_a} \delta^2(x - z_a(\tau_a)) \tag{5}$$

and is conserved. We observe that (2) and (3) form a closed system of $N + 1$ equations for which one can solve for the single metric degree of freedom and the N degrees of freedom of the point masses. The evolution of the dilaton field is governed by the evolution of the point masses via (4). The left-hand side of (4) is divergenceless (consistent with the conservation of $T_{\mu\nu}$), yielding only one independent equation to determine the single degree of freedom of the dilaton.

The procedure for casting the action and equations of motion has been discussed elsewhere [7–9]. We find for the action

$$I = \int d^2x \left\{ \sum_a p_a \dot{z}_a \delta(x - z_a) - \mathcal{H} \right\}, \tag{6}$$

where the reduced Hamiltonian is

$$H = \int dx \mathcal{H} = -\frac{1}{\kappa} \int dx \Delta\Psi, \tag{7}$$

where $\Delta \equiv \partial^2/\partial x^2$, and $\Psi = \Psi(x, z_a, p_a)$ and is understood to be determined from the constraint equations which are now

$$\Delta\Psi - \frac{(\Psi')^2}{4} + \kappa^2\pi^2 - \frac{\Lambda}{2} + \kappa\sum_a \sqrt{p_a^2 + m_a^2}\,\delta(x - z_a) = 0, \tag{8}$$

$$2\Delta\chi + \sum_a p_a \delta(x - z_a) = 0, \tag{9}$$

where $\pi = \chi' = \frac{d\chi}{dx}$ and π is the conjugate momenta to γ. The consistency of this canonical reduction has been demonstrated in previous work [11].

III. SOLVING THE CONSTRAINT EQUATIONS

The procedure for solving the constraints for $N = 3$ is similar to that for the $\Lambda = 0$ case [8,9]. We divide the space into four regions chosen so that $z_1 < z_2 < z_3$ and solve (8) and (9) exactly in the empty spaces between particles. Matching the fields at each of the particle positions, and ensuring that derivatives are consistent with integration of Eq. (8), yields the determining equation

$$\begin{aligned}&[((\hat{M}_1 + \hat{K}_1)(\hat{M}_3 + \hat{K}_4)\hat{M}_2 + (\hat{M}_1 + \hat{K}_1)\hat{K}_3^2 + (\hat{M}_3 + \hat{K}_4)\hat{K}_2^2)\tanh(\tfrac{1}{4}\hat{K}_3 z_{32})\tanh(\tfrac{1}{4}\hat{K}_2 z_{21})\\ &\quad + ((\hat{M}_1 + \hat{M}_2 + \hat{K}_1)(\hat{M}_3 + \hat{K}_4) + \hat{K}_3^2)\hat{K}_2\tanh(\tfrac{1}{4}\hat{K}_3 z_{32})\\ &\quad + ((\hat{M}_1 + \hat{K}_1)(\hat{M}_2 + \hat{M}_3 + \hat{K}_4) + \hat{K}_2^2)\hat{K}_3\tanh(\tfrac{1}{4}\hat{K}_2 z_{21}) + (\hat{M}_1 + \hat{M}_2 + \hat{M}_3 + \hat{K}_1 + \hat{K}_4)\hat{K}_2\hat{K}_3] = 0,\end{aligned} \tag{10}$$

where we impose the condition that the Hamiltonian

$$H = -\frac{1}{\kappa}\int dx\,\Delta\Psi = \frac{4}{\kappa}\sqrt{\kappa^2 X^2 - \frac{\Lambda}{2}} \tag{11}$$

remains finite as $x \to \infty$, where X is a constant of integration that comes from the solution of (9). The quantities in (10) are

$$\begin{aligned}\hat{M}_i &= \kappa\sqrt{p_i^2 + m_i^2},\\ \hat{K}_j &= -2\sqrt{\kappa^2\Big[X + \frac{\epsilon}{4}\Big(\sum_{i=1}^{3}\sigma_{ji}p_i\Big)\Big]^2 - \frac{\Lambda}{2}},\end{aligned} \tag{12}$$

where $\sigma_{ji} = -1$ when $j \le i$ and $\sigma_{ji} = 1$ when $i < j$. The parameter $\epsilon = \pm 1$ is a discrete constant of integration whose physical interpretation we discuss in the next section. Without loss of generality, we choose the center of inertia frame $p_1 + p_2 + p_3 = 0$, for which only the terms $\hat{K}_2$ or $\hat{K}_3$ can be imaginary. Consequently (10) is either purely real, or purely imaginary (in which case the i can be factored out). Permutation of the particles results in the exact same determining equation with the indices appropriately switched.

The Hamiltonian H is only implicitly determined from (10). Fortunately we do not need its explicit form since we can implicitly take derivatives on both sides of the determining Eq. (10) with respect to the phase space variables and from there extract the canonical equations of motion. From (11) with $p_Z = \sum_{a=1}^{3} p_a = 0$, we obtain

$$\frac{\partial H}{\partial x_k} = \frac{4}{\kappa}\Big(\frac{\partial}{\partial x_k}\sqrt{\kappa^2 X^2 - \frac{\Lambda}{2}}\Big) = \frac{4\kappa X}{\sqrt{\kappa^2 X^2 - \frac{\Lambda}{2}}}\frac{\partial X}{\partial x_k}, \tag{13}$$

where x_k is any of the canonical variables. We then have the simple but tedious task of taking $\frac{\partial}{\partial x_k}$ of both sides of Eq. (10), collecting the derivatives of X, and then converting them to derivatives of H via (13). This yields the canonical equations of motion

$$\dot{z}_a = \frac{\partial H}{\partial p_a}, \qquad \dot{p}_a = -\frac{\partial H}{\partial z_a}, \tag{14}$$

where the dot denotes a derivative with respect to the coordinate time. These equations of motion are straightforward but highly tedious to calculate and will not be included here. When calculating the equations of motion for the particles when they are not in the arrangement $z_1 < z_2 < z_3$ we temporarily change the labels of the particles so that they do satisfy this condition. This allows us to use the derivatives of (10) to calculate the equations of motion for each of the particles, after which the original particle labels are returned. This method works regardless of whether or not the particles are identical.

IV. SOLVING THE EQUATIONS OF MOTION

We can now numerically calculate the equations of motion for each of the three particles. This would give us six equations of motion when our physical system only has four effective degrees of freedom: two relative separations and their two conjugate momenta. Introducing the new variables

$$\begin{aligned}z_2 - z_1 &= \sqrt{2}\rho,\\ -(z_1 + z_2) + 2z_3 &= \sqrt{6}\lambda,\\ z_1 + z_2 + z_3 &= Z,\end{aligned} \tag{15}$$

we construct their conjugate momenta

$$p_\rho = \frac{1}{\sqrt{2}}(p_2 - p_1),$$
$$p_\lambda = \frac{1}{\sqrt{6}}(-(p_1 + p_2) + 2p_3), \tag{16}$$
$$p_Z = \frac{1}{3}(p_1 + p_2 + p_3),$$

which have been chosen to satisfy the canonical commutation relations $\{q_i, p_j\} = \delta_{ij}$. This choice of variables gives the Hamiltonian an explicit sixfold symmetry. We can set the conjugate variables Z and p_Z to arbitrary values since Z is irrelevant in our equations and we can fix the center of inertia by setting $p_Z = 0$ without loss of generality. This choice of variables allows us to write the determining equation in terms of only $\{\rho, \lambda, p_\rho, p_\lambda\}$ for a given cosmological constant. In this way, the relativistic Hamiltonian can be regarded as a function $H = H(\rho, \lambda, p_\rho, p_\lambda)$.

We see from this perspective that the linear three-particle system is equivalent to a single particle moving in a two-dimensional "potential well." This allows the variables $\rho, \lambda, p_\rho, p_\lambda$ to be interpreted as the coordinates and the conjugate momenta of this single particle, which we call the hex-particle due to the hexagonal symmetry of the potential. In the Newtonian case, the potential takes on the shape of a hexagonal-shaped cone with planar sides and is independent of the momenta [12]. The relativistic potential well is obtained by regarding the potential to be the difference between the Hamiltonian and the relativistic kinetic energy

$$V(\rho, \lambda)|_{p_\rho = a, p_\lambda = b} = H(\rho, \lambda, p_\rho = a, p_\lambda = b) - \sqrt{(mc^2)^2 + (c|p|)^2} \tag{17}$$

and is dependent on the momentum $|p| = \sqrt{a^2 + b^2}$ of the hex-particle as well as its position in the (ρ, λ) plane.[1] At a certain critical value, which we denote by V_{Rc}, the walls of the potential well curve in on themselves rendering the system intrinsically nonperturbative.

Since both X and H must be real, Eq. (11) implies

$$H \geq \frac{4}{\kappa}\sqrt{-\frac{\Lambda}{2}}$$

resulting in a negative critical value for Λ

$$\Lambda_{\text{negcrit}} = -\frac{H^2\kappa^2}{8}. \tag{18}$$

As $\Lambda \to \Lambda^+_{\text{negcrit}}$, we see that $X \to 0$. From Eq. (13) all of the derivatives of H tend to zero, rendering the hex-particle motionless. We have not been able to identify analytically the positive critical value of Λ. Rather we identify it numerically: when running simulations with Λ too large the three-particle system breaks out of its bound state, and our simulation breaks down. We have not yet been able to conclusively find why the system fails where it does, but we believe it may be due to the fact that, when radial momentum is present in the hex-particle system, a positive cosmological constant seems to lower the value of V_{Rc}, rendering the system intrinsically nonperturbative where it was previously in a perturbative regime. This hypothesis is supported by the fact that, for the energies that we have tested, the maximum value of Λ allowed seems to decrease substantially as H increases.

The effect on the hex-particle's orbits from approaching these positive and negative critical values of the cosmological constant will be further discussed in later sections.

There is no closed-form solution for either the determining Eq. (10) or to the equations of motion so we must solve these equations numerically. Introducing dimensionless variables $p_i = M_{\text{tot}}\hat{p}_i$ and $z_i = \frac{4}{\kappa M_{\text{tot}}}\hat{z}_i$, and rescaling X, H, and Λ, it is easy to show the determining equation and its derivative equations of motion can be written with $\kappa M_{\text{tot}} = \kappa\sum_{a=1}^{3} m_a$ set equal to unity. In practice it is easier to study the equal-mass three-body system by analyzing the motion of the hex-particle in the (ρ, λ) plane. In this system the bisectors joining opposite vertices of the potential well correspond to two of the three particles crossing one another, causing a discontinuous change in the hex-particle's acceleration. Therefore, in the Hamiltonian formalism, the motion of the hex-particle is governed by a pair of differential equations which are continuous everywhere except at the three hexagonal bisectors $\rho = 0$, $\rho - \sqrt{3}\lambda = 0$, and $\rho + \sqrt{3}\lambda = 0$. These correspond to the crossings of particles 1 and 2, 2 and 3, or 1 and 3, respectively.

We allow the hex-particle to freely cross over each of these bisectors, which corresponds to a pair of particles passing through each other. An analogous system in the Newtonian case consists of the motions of a ball under a constant gravitational force elastically colliding with a wedge [13]. This system is nearly identical to the one we study insofar as, in the equal-mass case, an elastic collision between a pair of particles in the three-body system cannot be distinguished from a crossing of two equal-mass particles. However, a distinction between the two systems in a certain class of orbits has been previously observed [8].

As with the $\Lambda = 0$ case the nonsmoothness of the potential gives rise to interesting dynamics rooted in two distinct types of motion [13]: A motion, which corresponds to the same pair of particles crossing twice in a row in the three-body system (or equivalently the hex-particle crossing a single bisector twice in succession), and B motion, in which a single particle crosses both of the other particles in succession (or equivalently the hex-particle crossing two successive hexagonal bisectors). For a given orbit we can

[1]Note that earlier definitions of the potential [8] defined it to be the value of the Hamiltonian at zero momenta.

characterize the motion by a sequence of these symbols with a finite exponent n denoting n repeats and an overbar denoting an infinite repeated sequence. It is important to note that the classification of a crossing as A or B motion is dependent on the previous crossing, so there is an ambiguity in the classification of either the final or the initial crossing. This is resolved by taking the initial crossing as unlabeled; since we are considering large sequences of motion this ambiguity causes no practical difficulties [8].

There is a technical difficulty in comparing trajectories in systems with different values for the cosmological constant. Such changes induce a change in the determining equation and so we cannot use exactly the same initial conditions. We will deal with this by comparing trajectories with the same fixed-energy initial conditions. This is done by fixing the initial values of H, ρ, λ, and p_ρ, and adjusting p_λ so that the Hamiltonian constraint is satisfied.

To study the motion of the system we can employ three methods of analysis. One is to plot the trajectory of the hex-particle in the (ρ, λ) plane and compare the motion under different initial conditions and in systems with a different value for the cosmological constant. Another is to plot the motion of the three particles as a function of time which gives us a different method for visualization, allowing us to identify differences in the various types of motion. Finally, we can construct Poincaré sections by plotting the radial momentum p_R, against the square of the angular momentum p_θ^2 of the hex-particle each time it crosses one of the bisectors. When all particles have equal mass, all of the bisectors are equivalent so all of the crossings can be plotted on the same surface of section. This allows us to easily identify regions of periodicity, quasiperiodicity, and chaos, and we will discuss each of these features.

We numerically integrate the equations of motion generated from the determining Eq. (10) using a MatLab ODE routine (ODE45 or ODE113). In order to control errors, we imposed absolute and relative error tolerances of 10^{-8} for the numerical ordinary differential equation (ODE) solvers. For the values of H we studied this yielded numerically stable solutions. We tested this by checking that the energy in the system remained constant throughout the motion to a value no larger than 10^{-6}.

In the present work we have taken all three particles to have equal mass, maintaining the hexagonal symmetry of the potential. As with the $\Lambda = 0$ case [8] we find three general classes of orbits which we denote as annulus, pretzel, and chaotic. Examples of these classes of orbits have been found at all energies and in the presence of a positive and negative cosmological constant. Furthermore, in each class there are orbits that eventually densely cover the region of the (ρ, λ) space that they occupy and orbits that do not. The latter situation corresponds to a regular orbit that repeats itself after a finite time—the symbol sequence consists of a finite sequence repeated infinitely many times, resulting in a periodic trajectory. The former situation corresponds to an orbit where the same finite sequence is repeated, but with a motion added or removed at irregular intervals, resulting in a quasiperiodic trajectory. The quasiperiodic orbits closely resemble the periodic orbits, except that they fail to exactly repeat themselves and have some form of precession that causes the orbits to fill a region of space. Thus these quasiperiodic orbits show a high degree of regularity, manifest by its periodic symbol sequence.

Chaotic orbits are those in which the hex-particle wanders between A motion and B motion in a seemingly irregular fashion. We identify them by localizing their initial conditions in a destroyed KAM region, as discussed in the next section. On the Poincaré section these orbits appear as densely filled regions. These orbits eventually wander into all areas of the (ρ, λ) plane allowed by the energy constraint, a trait not seen in either the annuli or pretzel orbits. Areas of chaos can be found in this system at the transition point between annulus and pretzel orbits, though the size of the chaotic region seems to be highly dependent on the cosmological constant, as will be shown later.

Since the diagrams that emerge from our analysis of trajectories in the (ρ, λ) plane and the plots of the motion of the three particles as a function of time are qualitatively similar to the $\Lambda = 0$ case, we shall omit their presentation here and turn to the construction of Poincaré sections.

V. POINCARÉ PLOTS

We now consider the Poincaré sections for this system. These are constructed by plotting the square of the angular momentum, p_θ^2 of the hex-particle against its radial momentum, p_R, each time it crosses one of the bisectors. Since we are looking only at the case when all three particles have the same mass, all of the bisectors are equivalent, and so we can plot all of the crossings on the same surface of section. This allows us to find regions of periodicity, quasiperiodicity, and chaos.

Since the trajectories of integrable systems can never intersect, there are severe limitations on the types of motion we observe. By definition they are comprised of the intersection of two two-dimensional surfaces, and so they will always appear as lines or dots for quasiperiodic and periodic orbits, respectively, on the Poincaré section. The extra degree of freedom present in completely nonintegrable systems permits an orbit to visit all regions of phase space, and the system typically displays strongly chaotic behavior. Such trajectories appear as filled-in areas on the Poincaré map.

When an integrable system is given a sufficiently small perturbation, most of its orbits remain confined to two-dimensional surfaces. However, it is possible that small areas of chaos will appear sandwiched between the remaining two-dimensional surfaces, which can grow as the magnitude of the perturbation is increased, eventually

becoming connected areas on the Poincaré section. This phenomenon is called a Kolmogorov-Arnold-Moser (KAM) transition [14]. Within these regions, islands of regularity may remain for quite some time and can have an intricate fractal structure [15], but the system will typically become almost fully ergodic for sufficiently large perturbations [16]. We identify chaotic orbits by localizing their initial conditions in a destroyed KAM region.

The outer bound of the Poincaré section is limited by the energy of the system. The first noticeable feature is that it is not symmetric about the $p_R = 0$ axis, but is instead skewed to the right, with the deformation increasing with H. This is at first puzzling; the trajectories of a subset of the annulus orbits always have positive radial velocities when they intersect one of the hexagon's edges and the tendency of all annulus orbits is to have $p_R > 0$ at the bisectors. However, it occurs because the Hamiltonian given by (10) is not invariant under the discrete symmetry $p_i \rightarrow -p_i$, but is only invariant under the weaker discrete symmetry $(p_i, \epsilon) \rightarrow (-p_i, -\epsilon)$. The parameter $\epsilon = \pm 1$ is a discrete constant of integration that is a measure of the flow of time of the gravitational field relative to the particle momenta. In our study we have chosen $\epsilon = +1$ throughout, which has the effect of making the principal features of the Poincaré plot "squashed" towards the lower right-hand side of the figure. If we had chosen $\epsilon = -1$ this deformation would be towards the lower left side. This is reminiscent of the situation for two particles, in which the gravitational coupling to the kinetic energy of the particles causes a distortion of the trajectory from an otherwise symmetric pattern [17,18] becoming more pronounced as H increases.

The general structure of the Poincaré section can be seen in Fig. 1. There is a fixed point just right of the center of the

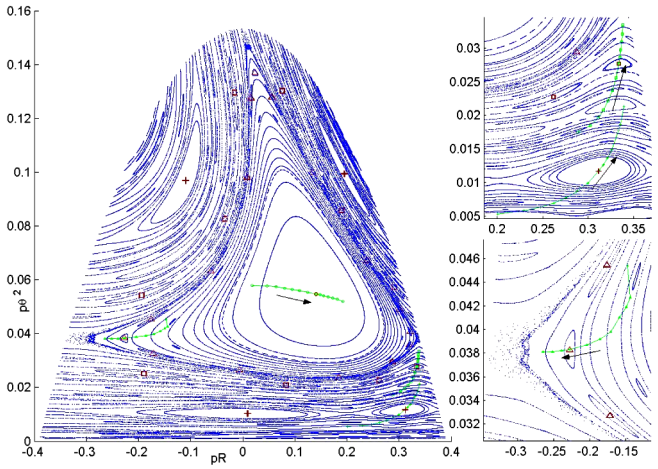

FIG. 1 (color online). Poincaré plot for $H = 1.2$ that tracks each of orbits (a -d) as described in the text. The curves indicate the trajectory of these orbits in the plot as Λ changes from -0.175 to 0.6, with the arrow indicating the direction of increasing Λ. The plot itself is for $\Lambda = 0$; the insets show close-ups of the trajectories near chaotic regions.

plot surrounded by triangular rings. These near-integrable curves correspond to the annulus orbits for that energy. All of the possible annulus orbits are contained in the largest triangular ring surrounding this region. Its boundary contains a thin region of chaos and outside of that, at the bottom and top corners, we have the regions corresponding to the pretzel orbits.

The structures in the lower part and upper corners of the Poincaré section is extremely complicated. We find a self similarity in these regions with a series of circles bounding the quasiperiodic near-integrable regions repeating themselves on increasingly smaller scales. We find that each of these circular patterns corresponds to a family of pretzel orbits. The two largest circles just below the annulus region correspond to the boomerang-shaped orbits ($\overline{AB^3}$). The next set of three circles corresponds to the sequence ($\overline{A^2B^3}$), and so on. We see a collection of crescents between these sets of circles and they correspond to the sequences $\overline{AB^3A^2B^3}$, $\overline{AB^3AB^3A^2B^3}$, and so on. Inside these circles there is actually a continuum of possible circles with a diameter that depends upon the initial conditions. These circles are centered around a single point that corresponds to the periodic orbit that these orbits approach.

As H increases, we remarkably do not find a breakdown from regular to chaotic motion in this system. As described before we see the plot skewed farther to the bottom right with larger H but the topology of the system seems to remain the same. For instance in the lower region of the Poincaré map we see the same patterns of series of circles at all different energies with no sizeable connected areas of chaos. We see the characteristic regions of chaos appearing in the regions between the annulus region and the pretzel orbits, but we see little change in the relative sizes of the chaotic regions with H.

When we introduce a negative cosmological constant we see some significant changes in the characteristics of the Poincaré sections shown in Fig. 2. First, we see that the asymmetric skewing of the graph to the bottom right is reduced and "pushed" back to the center. Specifically as Λ approaches its negative critical value, the Poincaré section becomes symmetric about the $p_R = 0$ line. In the bottom pretzel region we see that the repeating pattern of circles is continued but again centered on the graph instead of skewed to the right. This is similar to the low energy Newtonian case studied in [8] where the Poincaré section is also centered around $p_R = 0$. This is commensurate with the interpretation that the negative critical value of Λ for a given energy corresponds to the point where all of the energy in the system is vacuum energy, leaving no (i.e. very little) energy left for the motion of the particles.

The most surprising feature of the Poincaré section when $\Lambda < 0$ is the rapid disappearance of all the regions of chaos. In the region between the annulus and pretzel regions we find that once-chaotic orbits split into purely annulus or purely pretzel class orbits as Λ approaches its

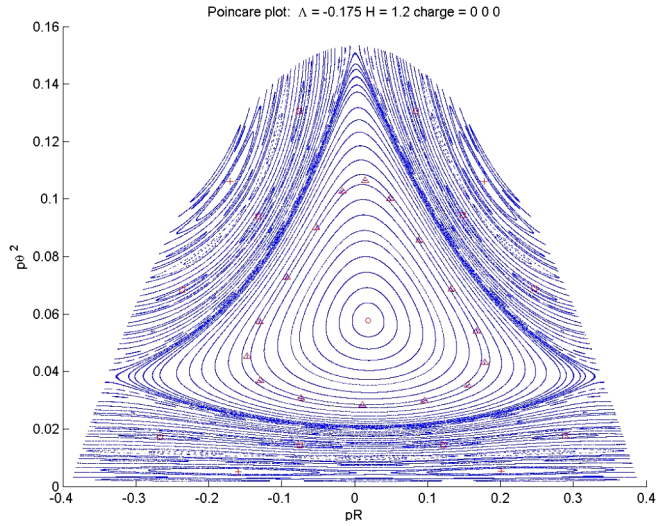

FIG. 2 (color online). Poincaré plot for $H = 1.2$ and $\Lambda = -0.175$, illustrating the locations of orbits (a-d).

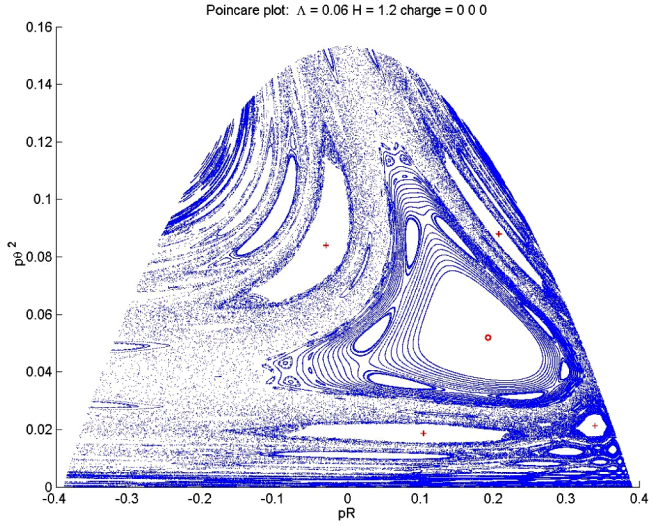

FIG. 3 (color online). Poincaré plot for $H = 1.2$ and $\Lambda = 0.06$, illustrating the locations of orbits (a) and (d); orbits (b) and (c) have become chaotic and so do not appear on the diagram.

negative critical value. We find no evidence of the onset of a KAM breakdown anywhere in the plot. This feature is strikingly different from what we have seen in the corresponding Newtonian system where chaos is present at all energies. Similar trends have been found at all numerically obtainable values of H.

In our study of the $\Lambda < 0$ case we were able to numerically solve the equations of motion of the hex-particle for all values of Λ up to the physical limit of the critical negative value where all of the energy of the system is ''used up'' in the contraction of the space-time. However, for the $\Lambda > 0$ case, due to the reduction of V_{rc} as Λ increases (as previously described) we find that the system that was in a perturbative regime quickly changes into an intrinsically nonperturbative system and our numerical simulations break down. This places much greater restrictions on what values of $\Lambda > 0$ we can test, especially at higher energies. Because of this numerical limit, our study of the $\Lambda > 0$ case is somewhat more restricted since we cannot follow the changes to this system up to a physical limit. However, we have seen the beginnings of a number of characteristic changes to the Poincaré section as Λ increases, as shown in Fig. 3.

First, many features are skewed farther to the right as Λ increases. Furthermore many of the features in the bottom pretzel region seem to be skewed up and to the right instead of down. Below the two large circles in the pretzel region we again see the repeating pattern of circles very well defined.

We also find that the chaotic region in between the boundary of the annulus and pretzel regions is also greatly increased, both in the corners of the boundary and along the sides. These characteristics are found at all numerically obtainable values of H, though for larger H, as described before we cannot increase Λ as much before the system becomes nonintegrable.

Furthermore, as Λ increases we at first see the onset of KAM breakdown in the pretzel region, followed by the appearance of major regions of chaos. For $H = 1.2$, at $\Lambda = 0.025$ some of the lines widen and small regions of chaos appear between the groups of ellipses. In these narrow regions the hex-particle seems to switch between orbits with an infinitely repeating symbol sequence (which correspond to the groups of ellipses) and orbits which undergo additional A type motions in quasiperiodic intervals (corresponding to the wavy lines) at seemingly irregular intervals. It is these regions that result in the chaotic pretzel orbits mentioned before. However, at this point most of the orbits still show very regular motions. As Λ increases to 0.05 these new regions of chaos expand around the groups of ellipses. Once we increase Λ to 0.06 most of the lower region of the Poincaré section becomes chaotic, with only a few nonconnected regions of regular motion remaining. This is in sharp contrast with the behavior of the system as Λ becomes negative, in which no evidence of any KAM breakdown is apparent. Although we have not been able to observe full KAM breakdown at all energies due to our previously mentioned limitations in studying systems with large Λ values, we have seen the initial trends that suggest the preliminary stages of KAM breakdown at higher energies.

We have also numerically studied how four different quasiperiodic (or stable) orbits, selected for their differing morphology, change as the cosmological constant Lambda changes. These are depicted in Figs. 1–3 as follows: (a) the stable (nearly circular) orbit located in the center of the annulus region (denoted by the $\circ$ symbol), (b) an annulus orbit located around the outside edge of the triangular annulus region (denoted by the $\triangle$ symbol), (c) a quasiperiodic pretzel orbit located halfway between the center of the

annulus region and the first large outer annulus regions (denoted by the $\square$ symbol), and (d) a banana-shaped AB^3 orbit located in the center of that region (denoted by the $+$ symbol). Note that orbits (b), (c), and (d) produce a set of points on the Poincaré plot that follow the contours of the triangular shaped region.

VI. DISCUSSION

Our investigation of the cosmological three-body problem has revealed a number of interesting features. We find in general that the presence of a cosmological constant significantly modifies the chaotic properties of the relativistic three-body system, and this in markedly different ways depending on its sign.

For a negative cosmological constant we find that there is a rapid decrease in the amount of chaos for all values of H that we were able to investigate. The size of the chaotic regions in the Poincaré plot are even smaller than in its nonrelativistic counterpart, despite the high degree of nonlinearity in the cosmological system. Indeed, as the cosmological constant approaches its negative critical value [defined in (18)], the chaotic regions nearly vanish. We conjecture that this occurs for arbitrarily large H, motivated primarily by our observation that the area of the chaotic regions in the Poincaré section seems to be roughly proportional to $|\frac{\Lambda}{\Lambda_{\text{negcrit}}}|$ for all energies we were able to numerically investigate.

Conversely, we find an increase in the area of chaotic regions in the Poincaré section when the cosmological constant is positive, both in the regions between the annulus and pretzel orbits, and within the regions corresponding to the pretzel orbits. Although we were unable to investigate large values of the cosmological constant at higher energies, we observed the lines in the pretzel regions of the Poincaré section starting to thicken as Λ increases and small regions of chaos appearing between the group of ellipses, reminiscent of the preliminary stages of KAM breakdown. We therefore conjecture that this increase in chaos occurs for positive Λ at all energies.

After numerically studying how certain stable orbits change as the cosmological constant changes we find that these orbits remain stable for $\Lambda < 0$ but for $\Lambda > 0$ stable orbits can become chaotic. The point of transition is dependent on the initial conditions of the orbit or its specific location in phase space. These results support the intuitive higher-dimensional understanding of a negative cosmological constant as a parameter that provides stronger gravitational binding, leading to an increase of the integrability of the dynamics and thus an increase in the stability of trajectories.

We close with some comments on future work. The unequal mass case remains to be explored. While we expect that the general feature of chaos increasing/decreasing with positive/negative Λ will still be present, there could be a number of surprising features in the details relative to the $\Lambda = 0$ case [9]. However, our primary limitation has been that of exploring energies that are below the critical value of the potential. This same limitation was present in previous studies of the $\Lambda = 0$ three-body system [8,9]—to move beyond it will require employing a time parameter that is not coordinate time, as well as more sophisticated numerical algorithms that avoid instabilities we encountered at higher energies.

ACKNOWLEDGMENTS

This work was supported by the Natural Sciences and Engineering Research Council of Canada.

[1] See the article by T. Damour in *Three Hundred Years of Gravitation*, edited by S. W. Hawking and W. Israel (Cambridge University Press, Cambridge, England, 1987).
[2] G. Rybicki, Astrophys. Space Sci. **14**, 56 (1971); H. L. Wright, B. N. Miller, and W. E. Stein, Astrophys. Space Sci. **84**, 421 (1982), and references therein.
[3] See B. N. Miller and P. Youngkins, Phys. Rev. Lett. **81**, 4794 (1998); K. R. Yawn and B. N. Miller, Phys. Rev. Lett. **79**, 3561 (1997), and references therein.
[4] R. B. Mann, Found. Phys. Lett. **4**, 425 (1991); Gen. Relativ. Gravit. **24**, 433 (1992).
[5] S. F. J. Chan and R. B. Mann, Classical Quantum Gravity **12**, 351 (1995).
[6] R. Jackiw, Nucl. Phys. **B252**, 343 (1985); C. Teitelboim, Phys. Lett. **126B**, 41 (1983).
[7] F. Burnell, R. B. Mann, and T. Ohta, Phys. Rev. Lett. **90**, 134101 (2003).
[8] F. J. Burnell, J. J. Malecki, R. B. Mann, and T. Ohta, Phys. Rev. E **69**, 016214 (2004).
[9] J. J. Malecki and R. B. Mann, Phys. Rev. E **69**, 066208 (2004).
[10] R. B. Mann, D. Robbins, and T. Ohta, Phys. Rev. D **60**, 104048 (1999); Phys. Rev. Lett. **82**, 3738 (1999).
[11] T. Ohta and R. B. Mann, Classical Quantum Gravity **13**, 2585 (1996).
[12] D. Bukta, G. Karl, and B. Nickel, Can. J. Phys. **78**, 449 (2000).
[13] H. E. Lehtihet and B. N. Miller, Physica D (Amsterdam) **20**, 93 (1986).
[14] V. I. Arnold and A. Avez, *Ergodic Problems of Classical Mechanics* (Springer, New York, 1968); A. N. Kolmogorov, Dokl. Akad. Nauk SSSR **98**, 527 (1954) [an English version can be found in *Proceedings of the 1954 International Congress of Mathematics* (North-

Holland, Amsterdam, 1957)]; V. I. Arnold, Russ. Math. Surv. **18**, 85 (1963); J. Moser, Nachr. Akad. Wiss. Goett. IIa, Math.-Phys. K1 **1**, 1 (1962).

[15] H. Koyama and T. Kinoshi, Phys. Lett. A **279**, 226 (2001); Europhys. Lett. **58**, 356 (2002).

[16] H. Reichl and R. Zheng, in *Nonlinear Resonance and Chaos in Directions in Chaos*, edited by B. Hao (World Scientific, Singapore, 1987).

[17] R. B. Mann and T. Ohta, Phys. Rev. D **55**, 4723 (1997); Classical Quantum Gravity **14**, 1259 (1997).

[18] R. B. Mann, D. Robbins, T. Ohta, and M. Trott, Nucl. Phys. **B590**, 367 (2000).